



Structural, Magnetic, and Electrical Properties of (1-x) Na_{0.5}Bi_{0.5}TiO₃–(x) NiFe₂O₄ (x = 0.1, 0.3, 0.5, 0.7, and 0.9) Multiferroic Particulate Composite

Shilpa Thakur¹ · Kusum Parmar¹ · Sarita Sharma¹ · N. S. Negi¹

Received: 15 July 2020 / Accepted: 23 September 2020 / Published online: 4 October 2020
© Springer Science+Business Media, LLC, part of Springer Nature 2020

Abstract

Multiferroic composites consisting of Na_{0.5}Bi_{0.5}TiO₃(NBT) and NiFe₂O₄(NFO) phases have been synthesized by using sol-gel and metal-organic decomposition (MOD) methods. The X-ray diffraction (XRD) and scanning electron microscopy (SEM) results confirm NBT and NFO phase formation in all composite samples without the presence of any intermediate phases. The phonon vibrational modes of the composite samples are detected by Raman spectroscopy over wavenumber regions from 100 to 1000 cm⁻¹ at room temperature. The dielectric constant and dielectric losses are measured over a wide range of frequencies from 1 kHz to 1 MHz at room temperature. Room temperature magnetization measurements confirm the ferromagnetic behavior of all the composite samples. The observed values of coercivity are significantly lower and lie between 9.5 and 49 Oe only, which signifies the soft magnetic behavior of samples. The highest leakage current density value (3.39×10^{-6}) has been observed for 50NBT-50NFO composite in I–V measurements. The present study reveals that NBT-NFO composites could be potential lead-free multiferroic composites and provide an alternative for designing environment-friendly devices.

Keywords X-ray diffraction · Composite · Magnetic hysteresis · Dielectric properties

1 Introduction

Multiferroics with magnetic and electric orders occurring simultaneously have received great research attention due to their wide range of technological applications such as multi-state memories, optical filters, phase shifters, microwave appliances and several other devices [1, 2]. The manipulation of magnetization by external electric field and variation of polarization in response to magnetic field show unexpected developments in conventional device applications. The multiferroic materials, based on their material constituents, are mainly divided into two classes: single-phase and multi-phase systems. However, the range of applications of single-phase materials has been limited because of weak ME response and low working temperature [3–5]. In order to exploit the combination between magnetic and electric fields, the artificial multiferroic

composites have been developed to achieve superior properties compared with those observed in the individual components [6, 7]. Multiferroic composites exhibit a strong magnetoelectric effect due to product property, which arises from coupling between magnetostrictive and piezoelectric effect in the ferromagnetic and ferroelectric phases respectively [8]. The magnetoelectric effect of magnetoelectric composites is different from single-phase multiferroic materials, which can be described as the deformation of the magnetic phase causes internal stress under the magnetic field, which is transmitted through the interface to the ferroelectric phase, producing polarization [9, 10]. The equilibrium composition of two phases i.e. ferroelectric and ferromagnetic composites has magnetoelectric coupling only when there is an induction of polarization with the application of magnetic field or magnetization and vice versa. It has been concluded that the ME effect is directly influenced by piezoelectric and magnetostrictive strengths or respective performance of ferroelectric and ferromagnetic phases respectively. It means that the coupling effect depends greatly on the properties of the respective components. Furthermore, the concept of composite materials having piezoelectric and magnetic coexisted phases such as BiFeO₃–Pb(Zr_{0.52}Ti_{0.48})O₃ [11], Pb_{0.99}[Zr_{0.45}Ti_{0.47}

✉ Shilpa Thakur
Shilpathakur22@yahoo.in

¹ Department of Physics, Himachal Pradesh University, Shimla, HP, India

$(\text{Ni}_{1/3}\text{Sb}_{2/3})_{0.08}\text{O}_3\text{-CoFe}_2\text{O}_4$ [12], and $(x)\text{Ni}_{0.8}\text{Zn}_{0.2}\text{Fe}_2\text{O}_4 + (1-x)\text{PZT}$ [13] has been reported. Although, due to health- and environment-related issues posed by lead-based composites, the focus has been already shifted towards the development of lead-free ME composites [14]. One of the most studied lead-free piezoelectric material, sodium bismuth titanate (NBT), is initially investigated by Smolenskii et al. in 1960 [15]. NBT is A-site complex structure having general formula $\text{AA}'\text{BO}_3$, where Na^+ and Bi^{3+} occupy A-site and Ti^{4+} occupies B-site of the unit cell. NBT shows strong ferroelectric properties at room temperature, piezoelectric coefficient value up to 73 pC/N, high remnant polarization, and maximum relative permittivity at 320 °C [16, 17]. Therefore, the NBT was chosen as the ferroelectric phase in the processing of environment-friendly multiferroic composites. Except for perovskites, spinel-type materials have also gained much attention because of their importance in technological applications. Nickel ferrite (NiFe_2O_4), a soft magnet with inverse spinel structure, is a well-studied ferrite compound with magnetic ordering temperature well above room temperature. Also, due to the large magnetostrictive coefficient, NFO is an interesting candidate for spin filtering tunnel barriers and spintronic devices. Structural and magnetic properties of NBT-CFO composite have also been reported in our previous publication [18]. Despite the fact that NiFe_2O_4 (NFO) has smaller magnetostriction than CoFe_2O_4 (CFO), NFO has high electrical resistivity, moderate saturation, low coercivity, and significant thermal and chemical stability [19]. S.N. Babu et al. [16] reported the synthesis of NBT-CFO composite and concluded that the NBT may be useful for designing lead-free composites with enhanced ME coupling effect. K. Praveena et al. [20] reported the synthesis of NBT- MnFe_2O_4 composites and observed that such composites are best suited for wide-band electrostatically tunable microwave devices. In this article, the synthesis and characterization of $(1-x)\text{Na}_{0.5}\text{Bi}_{0.5}\text{TiO}_3 - (x)\text{NiFe}_2\text{O}_4$ composites, containing sodium bismuth titanate ($\text{Na}_{0.5}\text{Bi}_{0.5}\text{TiO}_3$) as the ferroelectric component and nickel ferrite (NiFe_2O_4) as a ferromagnetic component, are presented. The structural, microstructural, dielectric, ferromagnetic, and electrical properties of NBT-NFO lead-free composite samples are reported in the following sections.

2 Experimental Details

$\text{Na}_{0.5}\text{Bi}_{0.5}\text{TiO}_3$ (NBT) was prepared by the sol-gel method. The stoichiometric amounts of bismuth nitrate ($\text{Bi}(\text{NO}_3)_3 \cdot 5\text{H}_2\text{O}$) and sodium nitrate (NaNO_3) dissolved gradually in acetic acid with continuous heating at 50 °C. Tetra-*n*-butyl orthotitanate ($\text{C}_{16}\text{H}_{36}\text{O}_4\text{Ti}$) mixed with acetylacetone was combined to the overhead mixture with continuous stirring at 60 °C temperature. The liquified citric acid was blended to the above solution by taking in 1:1.2

weight ratio. The final solution was heated at 50 °C to obtain the dry powder, which was further sintered at 1050 °C for 2 h to obtain NBT ceramic. (NiFe_2O_4) NFO powder was prepared by and metallo-organic decomposition (MOD) chemical solution method. To prepare (NiFe_2O_4) NFO powder, nickel-2-ethyl hexanoate $(\text{C}_7\text{H}_{15}\text{COO})_2\text{Ni}$ and iron-3-ethyl hexanoate $(\text{C}_7\text{H}_{15}\text{COO})_3\text{Fe}$ were prepared from the starting materials $\text{Ni}(\text{NO}_3)_2 \cdot 6\text{H}_2\text{O}$ and $\text{Fe}(\text{NO}_3)_3 \cdot 9\text{H}_2\text{O}$ respectively. The hexonates of Ni and Fe were mixed in the required stoichiometric ratio with continuous heating at 80 °C to obtain a dry powder of NFO. This dehydrated powder was sintered at 1050 °C for 2 h. Sodium bismuth titanate and nickel ferrite composites with the general formula $(1-x)\text{Na}_{0.5}\text{Bi}_{0.5}\text{TiO}_3 - (x)\text{NiFe}_2\text{O}_4$ ($x = 0.1, 0.3, 0.5, 0.7, \text{ and } 0.9$) and coded here after as 90NBT-10NFO, 70NBT-30NFO, 50NBT-50NFO, 30NBT-70NFO, and 10NBT-90NFO, respectively, were then prepared by mixing the NBT and NFO powders in stoichiometric concentration by using a mortar pestle. Then, 0.05% PVA was added as a binder and the powders were pressed under a hydraulic press into circular discs (pallets) of 10 mm diameter and a thickness of 2 mm at a pressure of 5 tones. These pallets were calcinated at 1100 °C for 2 h.

3 Results and Discussion

3.1 Structural Study

3.1.1 X-ray Diffraction

Figure 1 shows the X-ray diffraction (XRD) patterns of NBT, NFO, ceramics, and NBT-NFO composites sintered at 1050 °C for 2 h. The XRD pattern of NBT reveals the presence of rhombohedral perovskite crystal structure with space group R3c. The XRD pattern of NFO ceramic confirms the cubic spinel structure with space group Fd-3m. It can be seen that in ferrite structure (3 1 1) reflection is more intense, and in ferroelectric structures, the intensity of (1 1 0) reflection is maximum. No peak splitting is observed in the XRD image of NBT ceramics and the structure is nearly cubic. However, the presence of (021) peak near $2\theta \sim 40^\circ$ confirms the perovskite structure with a weak rhombohedral phase [21]. The XRD reflection lines corresponding to NBT (ferroelectric) and NFO (ferrite) constituent phases are well evolved in NBT-NFO composites for ferrite phase concentration up to $x = 0.7$. It means, no chemical reaction between NBT and NFO phases is visible. Nonetheless, the XRD figure of 10NBT-90NFO composite reveals a secondary phase near $2\theta \sim 33^\circ$. It can be noticed in XRD patterns that as the ferrite phase concentration increases, the intensity of ferrite peaks increases and that of ferroelectric peaks decreases. Thus, the number of diffraction peaks evolved and their intensity depends on the concentration of constituent phases in the

composite samples. The crystallite size was determined by using the Scherrer formula as given in Eq. 1 and the observed values are listed in Table 1.

$$D = \frac{k\lambda}{\beta \cos\theta} \tag{1}$$

Here, K is the dimensionless shape factor and its value is ~ 0.9 , λ is the X-ray wavelength, β is the full width at half maxima (FWHM), and θ is the Bragg angle. The lattice parameters corresponding to NBT and NFO phases in the composite samples differ slightly while comparing with those of pure NBT and NFO powder samples. The result also indicates that during the growth of composite samples, no third phase caused by chemical reaction occurs in both ferroelectric and ferromagnetic phases.

3.2 Raman Spectra

The phase transition behavior and local ionic configuration in the ceramics over a short range have been revealed by Raman spectra. According to group theory, due to disorder into A-site related to distorted octahedral $[\text{BiO}_6]$ and $[\text{NaO}_6]$ clusters, the NBT ceramics with rhombohedral structure are represented by $4A_1+9E$ with 13 Raman active modes, where A_1 and E modes are both Raman and infrared active [22]. Figure 2(a) shows the Raman spectra of NBT ceramic observed at room temperature over wavenumber range of 100 to 1000 cm^{-1} . The first Raman active mode at 127 cm^{-1} corresponds to the displacement of octahedral or network modifier $[\text{BiO}_6]$ and $[\text{NaO}_6]$ clusters. The second Raman active mode near 276 cm^{-1} is due to stretching arising from the bonds due to the presence of $[\text{TiO}]$ clusters at a short range. The third Raman active mode corresponds to short-range electrostatic force correlated with lattice ionicity. The TO_3 mode presents at 582 cm^{-1} is associated with $(-\text{O}-\text{Ti}-\text{O}-)$ symmetry vibrations of the octahedral $[\text{TiO}_6]$ cluster. This mode is usually seen in perovskite structure type materials. The modes observed at higher frequencies (764 and 844 cm^{-1}) may be

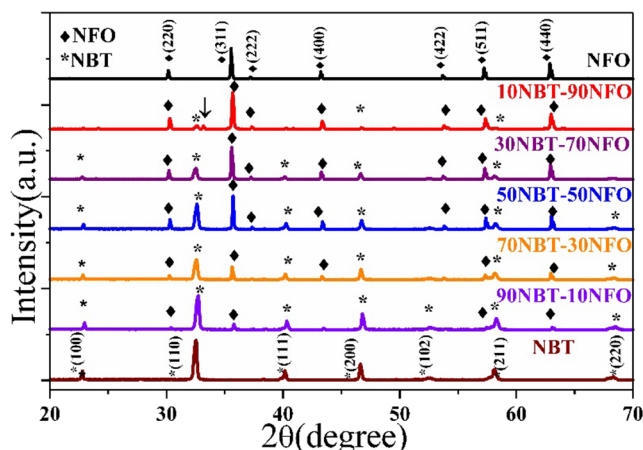


Fig. 1 X-ray diffraction patterns of NBT, NFO, and $(1-x) \text{Na}_{0.5}\text{Bi}_{0.5}\text{TiO}_3-x \text{NiFe}_2\text{O}_4$ ($x = 0.1, 0.3, 0.5, 0.7, \text{ and } 0.9$) composites

attributed to some oxygen defects. These modes can be divided into longitudinal and transverse components because of the electronic structure with the polar character of the lattice. The Raman spectra of all the composite samples are displayed in Fig. 2(b). It is noted that as the ferrite content increases, the intensity of the peaks goes on decreasing and no band is established after 50–50% composition. The behavior may be understood in terms of accidental degeneracy of phonon frequencies or insufficient intensities arising from the small polarizability of several modes in the ferrite phase.

3.3 Microstructural Study

Figure 3 shows the SEM images of NBT-NFO composite ceramic samples. The micrographs confirm the evolution of desired surface morphology in composites including grains of both constituent phases. The inhomogeneous dispersion of NBT and NFO grains can be seen in the micrographs. Thus, the surface morphological analysis confirms the presence of two different phases i.e. ferrite as well as ferroelectric in all composite samples. The average grain size of all the samples has been determined with Image J software and the observed values are listed in Table 1. The average grain size of both the

Table 1 Parameters calculated from XRD study and SEM micrographs

Samples	Crystallite size(nm)		Lattice parameter (Å)		Grain size(μm)	
	NBT	NFO	NBT	NFO	NBT	NFO
NBT	40	–	3.88	–	1.3	–
NFO	–	115	–	8.36	–	0.9
90NBT-10NFO	46	65	3.85	8.32	0.9	0.9
70NBT-30NFO	42	70	3.86	8.32	0.9	1.1
50NBT-50NFO	42	173	3.86	8.32	1.19	1.4
30NBT-70NFO	46	86	3.86	8.32	0.9	1.1
10NBT-90NFO	52	60	3.86	8.32	1.15	0.9

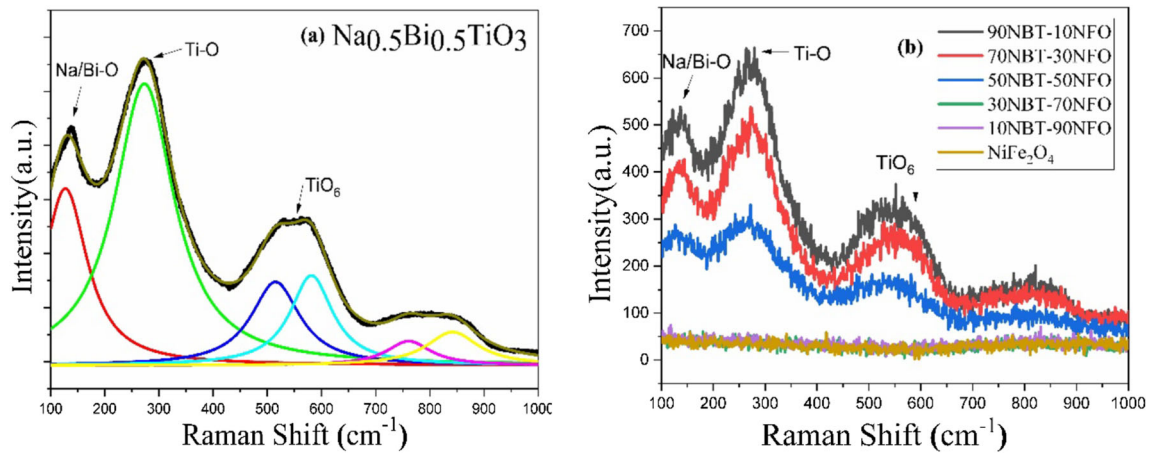


Fig. 2 Raman spectra of NBT ceramics (a) and Raman spectra of all the composite samples (b)

ferroelectric and ferrite phase lies in the range of 0.9 to 1.5 μm for all composite samples. It is known that in composites the distribution of ferrite and ferroelectric phases plays a most crucial role in the combination properties (magnetization, dielectric constant, resistivity, etc.) as well as in the coupling properties such as the ME output. A heterogeneous distribution or bimodal clusters of grains has been detected in the micrographs of composite samples. This may be because of the occupation of the grains of different sizes and phases (larger grains of ferroelectric and smaller of ferrite phases).

3.4 Magnetic Properties

The magnetization-magnetic field (M - H) curves of $(1-x)\text{Na}_{0.5}\text{Bi}_{0.5}\text{TiO}_3 - (x)\text{NiFe}_2\text{O}_4$ ($x=0.1, 0.3, 0.5, 0.7, \text{ and } 0.9$) multiferroic composites measured at room temperature by

using a vibrating sample magnetometer (VSM) under an applied magnetic field of ± 15 kOe are shown in Fig. 4. It is confirmed from the magnetic hysteresis loops that all the composite samples are magnetically soft at room temperature. The magnetic moment in terms of Bohr magneton of all the samples has been calculated by applying the formula given in Eq. 2 as

$$\mu_B = \frac{M \times \sigma S}{5582} \quad (2)$$

where M is the molecular weight, σ_s is the magnetization per gram mole of the sample, and 5585 is the magnetic factor. Also, the anisotropy constant is calculated using the formula

$$\text{Anisotropy constant}(K) = \frac{M_s \times H_c}{0.96} \quad (3)$$

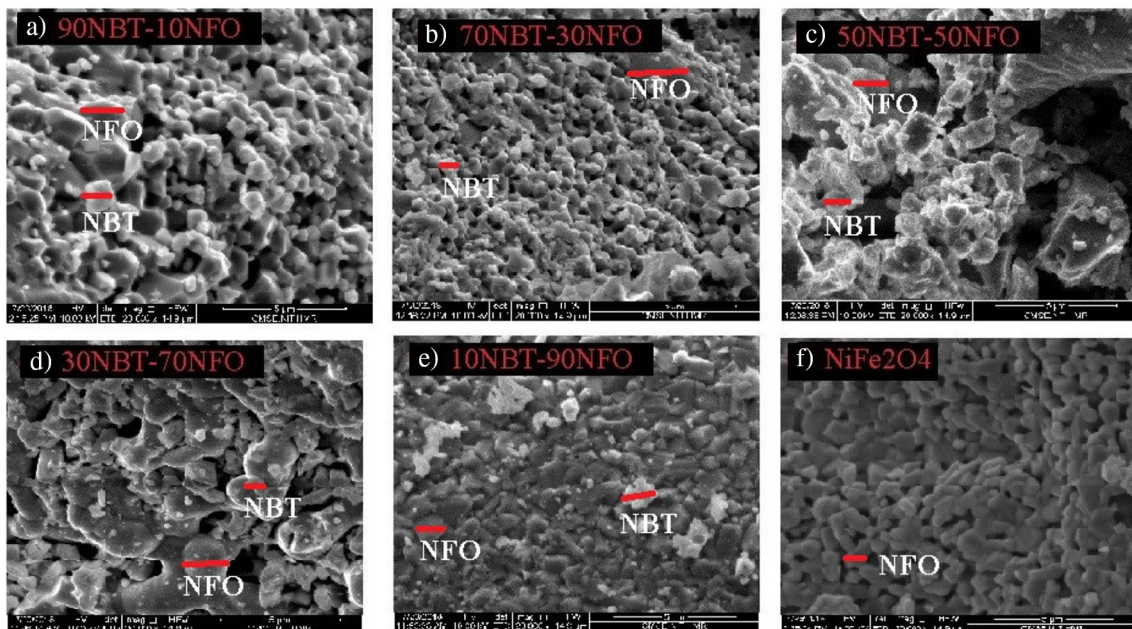


Fig. 3 a–e SEM micrographs of $(1-x)\text{Na}_{0.5}\text{Bi}_{0.5}\text{TiO}_3 - (x)\text{NiFe}_2\text{O}_4$ ($x=0.1, 0.3, 0.5, 0.7, \text{ and } 0.9$) composite and (f) NiFe_2O_4

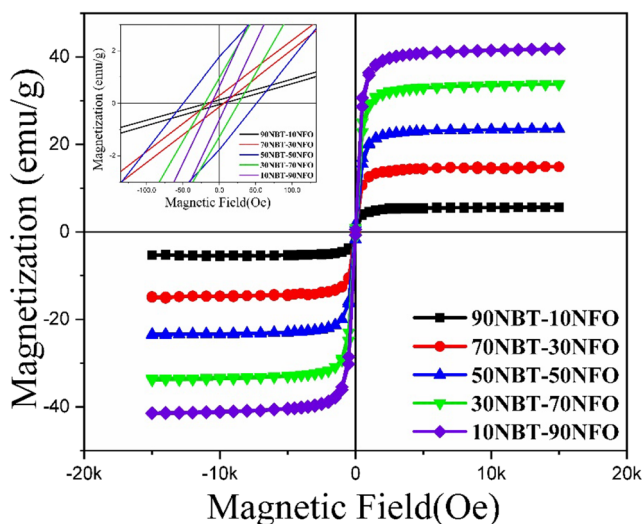


Fig. 4 M–H hysteresis loops of (1-x) $\text{Na}_{0.5}\text{Bi}_{0.5}\text{TiO}_3$ –(x) NiFe_2O_4 ($x = 0.1, 0.3, 0.5, 0.7, \text{ and } 0.9$) composite.

Here, M_s is the saturation magnetization, H_c is the coercivity, and 0.96 is a constant [23]. The saturation magnetization (M_s), remnant magnetization (M_r), squareness factor, coercivity (H_c), magnetic moment (μ_B), and anisotropy constant (K) are shown in Table 2. It can be seen from that that with accelerating ferrite phase concentration, the saturation magnetization values of composites enhance. This is due to the decrease in inclusion of the non-magnetic phase which reduces the magnetic interaction between ferrite grains. A non-symmetric behavior of coercive field (H_c) is observed with varying ferrite phase content. The coercivity values are very small and lie between 9.5 and 49 Oe only, signifying the soft magnetic behavior of these samples. High value of H_c is obtained for 50% of NiFe_2O_4 composition which may be by virtue of bad conduction of grain boundaries ascertained by SEM micrograph, results in domain wall pinning. Furthermore, high value of H_c for the composite is due to the existence of ferroelectric, as ferroelectric (piezoelectric) phase acts as the pinning center in the composite. The decrement in anisotropy constant after 50NBT-50NFO composition indicates that the dipoles of magnetic moments have a strong dependence in a particular direction. The values of the squareness factor (M_r/M_s) which is also known as reduced magnetization lie between 0 and 1 and are suitable for application in memory

devices. In general, if the value of squareness factor is greater than or equals to 0.5, materials are considered in a single magnetic domain structure and for values less than 0.5, the material exhibits a multidomain structure [24]. The value of the squareness factor of all the samples is less than 0.5 confirming the multidomain structure of all the composites. Also, the composite with 50–50% composition showing the highest value of M_r/M_s ratio suggests maximum magneto crystalline anisotropy which may be because of improvement in crystal order and structure.

3.5 Dielectric Study

The behavior of dielectric constant and loss tangent of (1-x) NBT-(x) NFO ceramic with different molar ratios as a function of frequency in the range of 1 KHz to 1 MHz at room temperature has been investigated and shown in Fig. 5(a) and (b). From Fig. 5(a), it can be clearly observed that the dielectric constant decreases with increasing frequency and showing dispersive behavior in the low-frequency region, while in the range of higher frequencies, the dielectric constant tends to remain stable. The behavior can be explained on the basis of the Maxwell–Wagner polarization theory and Koop’s two-layer model [25]. According to this model, a dielectric medium is supposed to be composed of disorderly conducting grain boundaries at low frequencies and highly conducting grains at high-frequency range. The large dielectric constant at low frequencies owing to space charge polarization is caused by inhomogeneous structure. At lower frequencies, all the polarization mechanisms such as dipolar, ionic, electronic, and interfacial polarization contribute towards permittivity but as frequency goes on increasing, only electron displacement mechanism contributes [26]. The dielectric constant values for (1-x) NBT-(x) NFO composites with x variation from 0.1 to 0.9 are 106, 1080, 1333, 1008, and 998 respectively observed at a frequency of 1 kHz. It is noticed that with the increase in ferrite concentration, the dielectric constant first increases for samples up to 50NBT-50NFO composition and then decreases. It can be found that uniformity of the sample with 50–50% composite is higher, confirmed via FESEM micrographs which leads to higher space charge polarization resulting in maximum

Table 2 Saturation magnetization (M_s), remnant magnetization (M_r), squareness factor (M_r/M_s), coercivity (H_c), magnetic moment (μ_B) and anisotropy constant (K) for (1-x)NBT-(x) NFO ($x = 0.1, 0.3, 0.5, 0.7$ and 0.9) system

Samples	M_s (emu/g)	M_r (emu/g)	M_r/M_s	H_c (Oe)	μ_B	K (erg/g)
90NBT-10NFO	5.68	0.08	0.01	10	0.20	59
70NBT-30NFO	14.85	0.20	0.01	9.5	0.51	146
50NBT-50NFO	23.71	1.76	0.07	49	0.78	1210
30NBT-70NFO	33.53	1.12	0.03	21	1.05	733
10NBT-90NFO	41.85	0.63	0.1	9.7	1.13	422

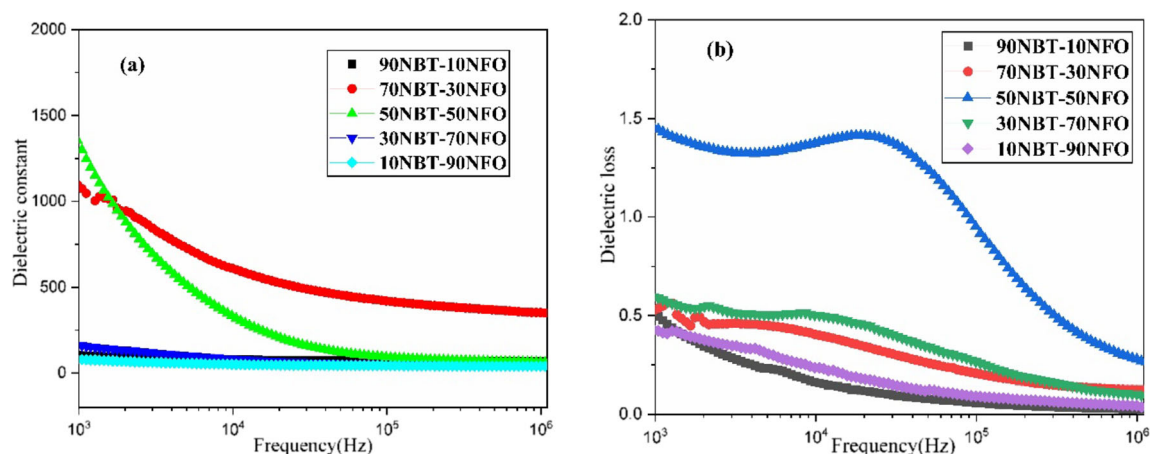


Fig. 5 Variation of dielectric constant (a) and dielectric loss (b) with the frequency of all the composite samples

dielectric constant. The dielectric loss is proportional to the imaginary part of the dielectric constant and expresses the dissipation of energy in the dielectric medium. The loss tangent values gradually decrease at beneath frequency range and nearly constant at higher frequency regions, i.e., at frequency $> 10^5$ Hz. The observed dielectric loss values at 1 kHz are 0.49, 0.49, 1.15, 0.58, and 0.41 for NBT-NFO composites with NFO concentration of 10, 30, 50, 70, and 90 mol% respectively. The behavior may be understood in terms of grain boundaries which are more efficacious at lower frequencies. A huge amount of energy is required for the exchange of electrons between ferrite ions followed by high dielectric losses. Also, the highly conducting grains are associated with higher frequency regions where a low energy dissipation occurs during the electron exchange process between ferrite ions [27].

3.6 Electrical Properties

The electrical properties such as conduction mechanism and leakage current behavior are significant to investigate for

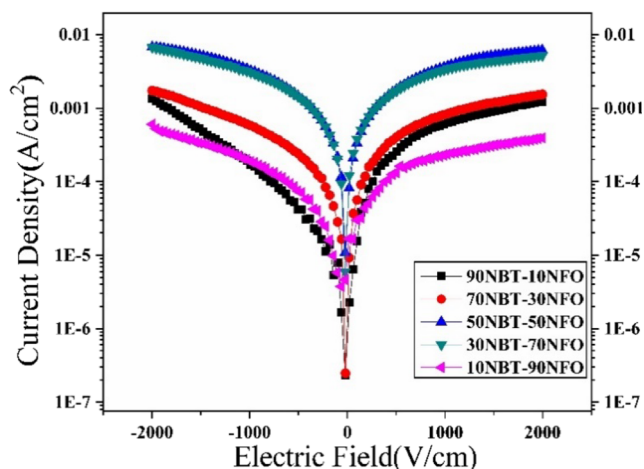


Fig. 6 Electric field vs. current density graph of all the composite samples

application of material in electronic devices. Figure 6 shows the leakage current characteristics of NBT-NFO composites under forward and reverse bias conditions measured at 200 V at room temperature. The J-E graph reveals that the leakage current density is directly proportional to the applied bias voltage confirming the ohmic behavior of samples in lower electric field regions. The observed conductivity values for $(1-x)$ NBT- (x) NFO ($x = 0.1$ to 0.9) composites are 5×10^{-7} , 7.57×10^{-7} , 3.39×10^{-6} , 3.04×10^{-6} , and $2.19 \times 10^{-7} \Omega^{-1} \text{cm}^{-1}$ respectively. The conductivity increases with NFO content up to for 50NBT-50NFO sample and decreases for samples with higher NFO phase content. Similar behavior is also noticed in dielectric characteristic measurements. The result may be attributed to large grain size which contributes towards leakage current density due to less scattering of charge carriers. Also, the highest value of leakage current density is observed for sample with 50% of NiFe_2O_4 concentration and is attributed to inhomogeneous distribution of grains as revealed in SEM micrographs.

4 Conclusion

In this work, $(1-x) \text{Na}_{0.5}\text{Bi}_{0.5}\text{TiO}_3 - (x) \text{NiFe}_2\text{O}_4$ ($x = 0.1, 0.3, 0.5, 0.7, \text{ and } 0.9$) composites were successfully prepared. The presence of both the parent compounds, i.e. ferroelectric NBT and ferrite NFO phases, in composite has been confirmed by XRD patterns and SEM micrographs. The well-saturated M-H hysteresis loops verify the ferromagnetic nature of all the multiferroic composites. The 50NBT-50NFO composition shows the highest value of dielectric constant and coercivity because of badly conducting grain boundaries confirmed by SEM micrograph.

Acknowledgments The authors are thankful to DST, New Delhi, India, for Inspire Fellowship (DST/INSPIRE Fellowship/2015/IF150783).

Compliance with Ethical Standards

Conflict of Interest The authors declare they have no conflict of interest.

References

- Fiebig, M.: TOPICAL REVIEW: revival of the magnetoelectric effect. *J. Phys. D: Appl. Phys.* **38**, 123–152 (2005)
- Chu, Z., PourhosseiniAsl, M.J., Dong, S.: Review of multi-layered magnetoelectric composite materials and devices applications. *J. Phys. D: Appl. Phys.* **51**, 243001 (2018)
- Schmid, H.: Some symmetry aspects of ferroics and single phase multiferroics. *J. Phys. Condens. Matter.* **20**, 434201 (2008)
- Pan, P., Tao, J., Ma, F., Zhang, N.: Magnetodielectric effect in $(1-x)(\text{Ba}_{0.88}\text{Ca}_{0.12})(\text{Ti}_{0.88}\text{Zr}_{0.12})\text{O}_3 - x\text{CoFe}_2\text{O}_4$. *J. Magn. Magn. Mater.* **453**, 91 (2018)
- Khomeriki, R., Chotorlishvili, L., Tralle, I., Berakdar, J.: Positive–negative birefringence in multiferroic layered metasurfaces. *Nano Lett.* **16**, 7290 (2016)
- Cheong, S.W., Mostovoy, M.: Multiferroics: a magnetic twist for ferroelectricity. *Nat. Mater.* **6**, 13–20 (2007)
- Trukhanov, S., Trukhanov, A.V., Kostishyn, V.G., Panina, L.V., Turchenko, V., Chushkova, D., Trukhanova, E.L., Viktor, O., Yakovenko, E.S., Matzui, L.: Magnetic, dielectric and microwave properties of the $\text{BaFe}_{12-x}\text{Ga}_x\text{O}_{19}$ ($x \leq 1.2$) solid solutions at room temperature. *J. Magn. Magn. Mater.* **442**, 300 (2017)
- Belavi, P.B., Chavan, G.N., Naik, L.R., Kotnala, R.K.: Grain size dependent dielectric and magnetic properties of $(Y)\text{NCCF} + (1 - Y)\text{BTO}$ particulate composites. *Int. J. Nanosci.* **11**(3), 1240007 (2012)
- Woldu, T., Raneesh, B., Hazra, B.K., Srinath, S., Padmanapan, S., Reddy, M.V.R., Kalarikkal, N.R.: A comparative study on structural, dielectric and multiferroic properties of $\text{CaFe}_2\text{O}_4/\text{BaTiO}_3$ core-shell and mixed composites. *J. Alloys Compd.* **691**, 644 (2017)
- Xu, R.C., Zhang, S.L., Wang, F.Q., Zhang, Q.W., Li, Z.D., Wang, Z.H., Gao, R.L., Fu, C.L.: The study of microstructure, dielectric and multiferroic properties of $(1 - x)\text{Co}_{0.8}\text{Cu}_{0.2}\text{Fe}_2\text{O}_4/x\text{Ba}_{0.6}\text{Sr}_{0.4}\text{TiO}_3$ Composites. *J. Electron. Mater.* **48**(1), 386 (2019)
- Xue, F., Tang, L., Guo, P., Luo, Z., Li, W.: Multiferroic properties of $\text{BiFeO}_3/\text{Pb}(\text{Zr}_{0.52}\text{Ti}_{0.48})\text{O}_3$ solid solution. *J. Mater. Sci. Mater. Electron.* **29**, 14285–14291 (2018)
- Schileo, G., Gonzalez, C.P., Alguero, M., Reaney, I.M., Postolache, P., Mitoseriu, L., Reichmann, K., Venet, M., Feteira, A.: Multiferroic and magnetoelectric properties of $\text{Pb}_{0.99}[\text{Zr}_{0.45}\text{Ti}_{0.47}(\text{Ni}_{1/3}\text{Sb}_{2/3})_{0.08}]\text{O}_3 - \text{CoFe}_2\text{O}_4$ multilayer composites fabricated by tape casting. *J. Eur. Ceram. Soc.* **38**, 1473–1478 (2018)
- Chougule, S.S., Chougule, B.K.: Studies on electrical properties and the magnetoelectric effect on ferroelectric-rich $(x)\text{Ni}_{0.8}\text{Zn}_{0.2}\text{Fe}_2\text{O}_4 + (1 - x)\text{PZT}$ ME composites. *Smart Mater. Struct.* **16**, 493–497 (2007)
- Saito, Y., Takao, H., Tani, T., Nonoyama, T., Takatori, K., Homma, T., Nagaya, T., Nakamura, M.: Lead-free piezoceramics. *Nature.* **432**, 84–87 (2004)
- Smolenskii, G.A., Isupov, V.A., Agranovskaya, A.I., Krainik, N.N.: New ferroelectrics of complex composition. *Sov. Phys. Solid State.* **2**, 2651–2654 (1961)
- Babu, S.N., Min, S.G., Malkinski, L.: Electric field tunable magnetic properties of lead-free $\text{Na}_{0.5}\text{Bi}_{0.5}\text{TiO}_3/\text{CoFe}_2\text{O}_4$ multiferroic composites. *J. Appl. Phys.* **109**, 07D911 (2011)
- Aksel, E., Jones, J.L.: Advances in lead-free piezoelectric materials for sensors and actuators. *Sensors.* **10**, 1935–1954 (2010)
- Naidu, K.C.B., Madhuri, W.: Microwave assisted solid state reaction method: investigations on electrical and magnetic properties NiMgZn ferrites. *Mater. Chem. Phys.* **181**, 432–443 (2016)
- Thakur, S., Parmar, K., Sharma, S., Negi, N.S.: Structural and electrical properties of $(1-x)\text{Na}_{0.5}\text{Bi}_{0.5}\text{TiO}_3 - x\text{CoFe}_2\text{O}_4$ ($x = 0.1, 0.2$) multiferroic composite ceramic. *Mater. Today Proc.* **28**, 115–118 (2020)
- Praveena, K., Varma, K.B.R.: Improved magneto-electric response in $\text{Na}_{0.5}\text{Bi}_{0.5}\text{TiO}_3 - \text{MnFe}_2\text{O}_4$ composites. *J. Mater. Sci. Mater. Electron.* **25**, 111–116 (2014)
- Kang, W.S., Koh, J.H.: $(1-x)\text{Na}_{0.5}\text{Bi}_{0.5}\text{TiO}_3 - x\text{BaTiO}_3$ lead free piezoelectric ceramics for energy harvesting applications. *J. Eur. Ceram. Soc.* **35**, 2057–2064 (2015)
- Niranjana, M.K., Karthik, T., Asthana, S., Pan, J., Waghmare, U.V.: Theoretical and experimental investigation of Raman modes, ferroelectric and dielectric properties of relaxor $\text{Na}_{0.5}\text{Bi}_{0.5}\text{TiO}_3$. *J. Appl. Phys.* **113**, 194106 (2013)
- Fonsecaa, S. G. C., Neivab, L. S., Bonifácio, M. A. R., dos Santos P. R. C., Silvad, U. C., de Oliveiraa, J. B. L.: Tunable magnetic and electrical properties of cobalt and zinc ferrites $\text{CO}_{1-x}\text{Zn}_x\text{Fe}_2\text{O}_4$ synthesized by combustion route. *Mater. Res.* **21**(3) 2018
- Saffari, F., Kameli, P., Rahimi, M., Ahmadvand, H., Salamati, H.: Effects of Co-substitution on the structural and magnetic properties of $\text{NiCo}_x\text{Fe}_{2-x}\text{O}_4$ ferrite nanoparticles. *Ceram. Int.* **45**(6), 7352–7358 (2015)
- Koops, C.G.: On the dispersion of resistivity and dielectric constant of some semiconductors at audio frequencies. *Phys. Rev. B.* **83**, 121 (1951)
- Murthy, V.R.K., Sobhanadri, J.: Dielectric properties of some nickel-zinc ferrites at radio frequency. *Phys. Stat. Sol. A.* **36**, K133 (1976)
- Kharabe, R.G., Devan, R.S., Kanamadi, C.M., Chougule, B.K.: Dielectric properties of mixed Li–Ni–Cd ferrites. *Smart Mater. Struct.* **15**, N36 (2006)

Publisher's note Springer Nature remains neutral with regard to jurisdictional claims in published maps and institutional affiliations.